Prompt Fission Neutron Investigation in $^{235}U(n_{th},f)$ and $^{252}Cf(sf)$ Reactions

Shakir Zeynalov, Pavel Sedyshev, Valery Shvetsov and Olga Sidorova

Joint Institute for Nuclear Research, 141980 Dubna, Moscow region, Russia

Abstract. The prompt neutron emission in thermal neutron induced fission of ^{235}U and spontaneous fission of ^{252}Cf investigated applying digital signal electronics. The goal was to check new revised data analysis software with fission fragment (FF) kinetic energy corrections after prompt fission neutron (PFN) emission. The revised software was used to reanalyze old data measured in EC-JRC-IRMM, where $^{252}Cf(sf)$ reaction was investigated. Both measurements were done using similar twin Frisch grid ionization chamber for fission fragment detection with NE213 equivalent fast neutron detector. In total about $0.5 \cdot 10^6$ FF with PFN coincidences have been analyzed in both measurements. The fission fragment kinetic energy, mass and angular distribution has been investigated along with prompt neutron time of flight and pulse shape analysis using a six channel synchronous waveform digitizer (WFD) with sampling frequency of 250 MHz and 12 bit resolution in $^{235}U(n_{th},f)$ reaction investigation. Similar WFD with sampling frequency 100 MHz was used for PFN investigation in $^{252}Cf(sf)$ reaction. These two experiments was considered as a reference for further investigations with a new setup composed of position sensitive ionization chamber as FF detector and array of 32 liquid scintillator PFN detectors recently constructed in Dubna.

1 Introduction

The nuclear fission is considered as the process of charged drop development under competition between attractive nuclear and repulsing coulomb forces, leading eventually to the split of the nucleus mainly into two parts of comparable masses. The main part of FF excitation energy is released by the prompt fission neutrons, emitted by FF after full acceleration by coulomb forces. The experimental investigations of various characteristics of PFN emission is needed to understand the nuclear fission dynamics from the scission point down to rupture. One of the interesting observation is the increasing $\bar{\nu}(A)$ from the heavy fragment with increase of the excitation energy of the fissioning system [1] still has no clear explanation. Therefore, further systematic study of correlations between fragments and neutron characteristics is needed. The studies of PFN emission in fission induced by neutrons from energies extending from resonances up to a few MeV could possibly contribute to better understanding the mechanism of PFN emission from the excited FF. The experiments on sub-barrier fission, induced by thermal neutrons are of particular interest because of no measurements was done so far on mass and energy distributions for this systems [2]. In this work we report results of PFN investigation in thermal neutron-induced fission of ^{235}U and spontaneous fission of ^{252}Cf. The main goal of the experiments was the feasibility check of the apparatus and data analysis procedure.

2 Experimental Setup and FF data analysis

A convenient way to study of PFN emission in neutron-induced fission is to use a conventional twin back-to-back ionization chamber, with two chambers sharing a common cathode as was done by Budtz-Jorgensen and Knitter [3]. The cathode was made from a thin

conductive foil and at the same time served as backing for the fissile deposit. For binary fission events two complementary FF are simultaneously detected in two independent chambers. Free electrons released by FF deceleration are induced pulses on the chambers anodes and on the common cathode during drift along the applied externally electric field. The pulse height in each chamber was proportional to corresponding FF kinetic energy release and the FF pulse shape conveys information on the FF angle (Θ) in respect to the electric field applied in the direction of the normal to the cathode plane. From the correlated energies obtained in the above double-energy (2E) experiment, FF masses and velocities could be found in the way similar to that in book [4]. If the fissile target is located on the common cathode and the fast neutron detector positioned at the certain distance along the normal to the target the angle between FF and PFN emission would be equal to Θ. The PFN velocity may be determined from the known flight path and the measured time delay between cathode and ND pulses. Measured FF and PFN velocity vectors then may be used for PFN emission kinematics. The PFN multiplicity distributions in respect to FF kinetic energy release and mass split may be reconstructed by comparison of two sets of FF measurements. In the first experiment fission fragment mass and kinetic energy release should be evaluated from the measurement independent from ND. In the second experiment FF mass and kinetic energy release should be evaluated for the FF coincided with ND. The detailed information on PFN emission in fission is available from the measured dependence of the number $\nu(A,TKE)$ of PFN emitted by the FF with mass number A and TKE release of two fission fragments [3-4]. The late function allowed obtaining of averaged characteristics on $\bar{\nu}(A)$ or $\bar{\nu}(TKE)$ by integrating over respective variable, if the mass yield matrix - *Y(A,TKE)* is known, for example:

$$\begin{aligned} \bar{\nu}(A) &= \frac{\int_0^\infty \nu(A,TKE)Y(A,TKE)dTKE}{\int_0^\infty Y(A,TKE)dTKE}, \\ \bar{\nu} &= \int_0^\infty \nu(A,TKE)Y(A,TKE)dTKEdA, \\ 200 &= \int_0^\infty Y(A,TKE)dTKEdA. \end{aligned} \tag{1}$$

Similar relation could be written for averaging over A:

$$\begin{aligned} \bar{\nu}(TKE) &= \frac{\int_0^\infty \nu(A,TKE)Y(A,TKE)dA}{\int_0^\infty Y(A,TKE)dA}, \\ \bar{\nu} &= \int_0^\infty \nu(A,TKE)Y(A,TKE)dTKEdA, \\ 200 &= \int_0^\infty Y(A,TKE)dTKEdA. \end{aligned} \tag{2}$$

$\nu(A),\nu(TKE)$ can be easily determined if the distributions of $P(A,TKE)$ and $Y(A,TKE)$ are known. The experimental method and data analysis procedure implemented in this work was adopted from Ref. [3], where it was described in detail. For each fission event the FF and PFN kinetic energies, FF masses along with the angle between PFN and FF motion should be determined. All this information can then be used to reconstruct the PFN emission kinematics both in the laboratory (LF) and in the centre of mass (CMF) frames. The measurements were carried out using the experimental setup presented in Fig. 1. Reaction kinematics is sketched is sketched Reaction kinematics is sketched in Fig. 2.

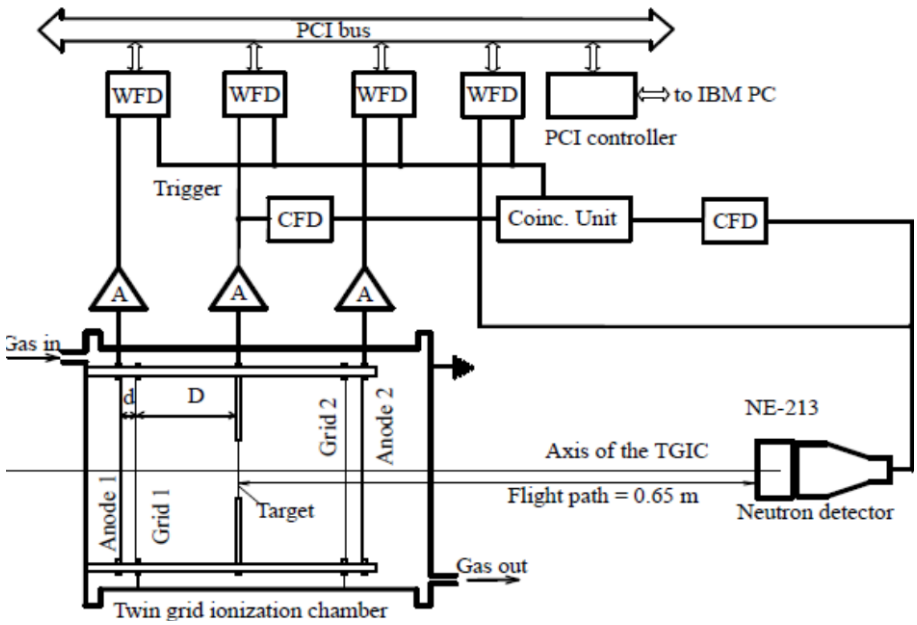

Fig. 1. Experimental Setup.

The experimental setup consisted of the twin back-to-back ionization chamber (TIC), which was designated for FF kinetic energy release and the cosine of angle between fission axis and the cathode plane normal measurement.

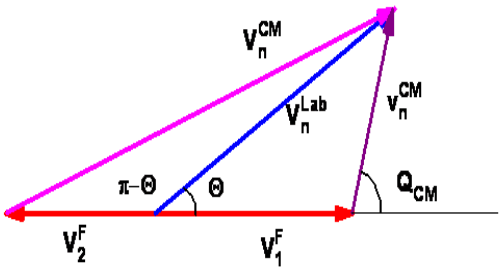

Fig. 2. Vector diagram for PFN emission from FF.

The experimental data was collected using a digital pulse processing (DPP) system, consisting of six synchronous waveform digitizers (12 bit, 250 MS/sec). The FF energies and angles were obtained from the chamber signal waveforms using DPP, realized in form of recursive procedures. The neutron energy was derived from time-of-flight (TOF) calculated as delay between the cathode and the neutron detector pulses. The measured FF energy release should be corrected for energy losses in the target layer and target backing if the cosine of angle Θ is known. In this work anode current pulse waveform was derived from the output pulse of charge sensitive preamplifier and the pulse "centre of gravity" (T) calculated as described in Ref. [5]. The relation between T and the cos(Θ) was derived in Ref. [6] using Ramo-Shokley theorem and numerically calculated weighting potentials:

$$\cos(\Theta) = (T_{90} - T)/(T_{90} - T_0), \tag{3}$$

where the used variables have the following meaning: D-is the cathode-anode distance, d - is the grid-anode distance, σ-is the Frisch grid inefficiency value, $T_0 = T(\cos(\Theta) = 1)$, $T_{90} = T(\cos(\Theta) = 0$. The below formula was used to correct anode signal pulse heights for grid inefficiency:

$$P_A^C = P_A / (1 - \sigma(1 - \frac{T}{T_{90}}) \cdot (1 + \frac{d}{2D})). \quad (4)$$

After the emission angle was calculated the average anode pulse height versus 1/cos(Θ) was plotted for both chambers to find energy loss correction for FF detected in each chamber. The data sets are fitted as a linear function of 1/ cos(Θ), the slopes of which were assigned to energy loss correction in respective chamber. The correction for FF pulse height caused by momentum transfer to working gas atoms by FF (non ionizing collisions) during its deceleration – is called pulse height defect (PHD). The PHD depends on the FF mass and kinetic energy and was corrected in data analysis using parameterization suggested in Ref. [6]:

$$E = \alpha \cdot PH + \beta + PHD(A_{post}, E_{post}), \quad (5)$$

where $E_{post}t$, A_{post} - FF kinetic energy and mass respectively after neutron emission. The fitting parameters α and β - are chosen to arrive at the values of *TKE* and $\langle A_H \rangle$ as given in Ref. [4] p. 323. After all corrections have been implemented we went to reconstruct the mass yield for investigated reaction. To do so we needed $\bar{\nu}(A)$ from literature and we used data from Ref. [8] and from Ref. [2]. The mass yield curve was obtained using $\bar{\nu}(A)$ for $^{235}U(n_{th},f)$ reaction from Ref. [2] is shown in Fig. 4 in comparison with result published in Ref. [4] p. 300.

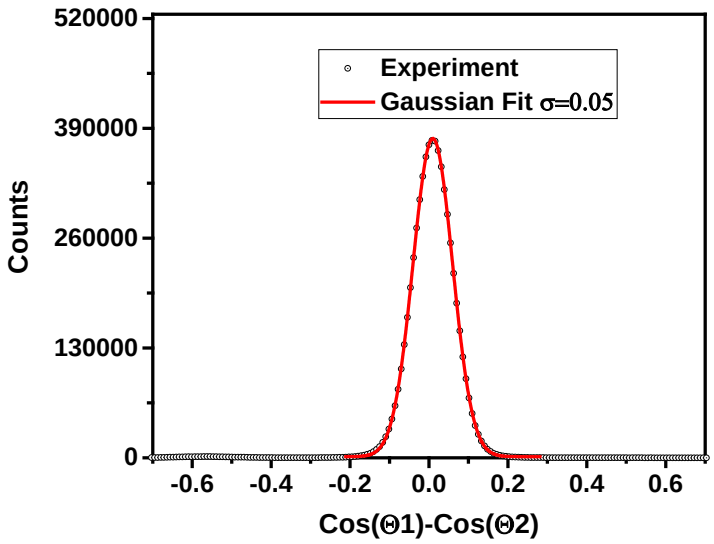

Fig. 3. Demonstration the precision of cos(Θ) measurement in the range 0.5<cos(Θ)<1.0.

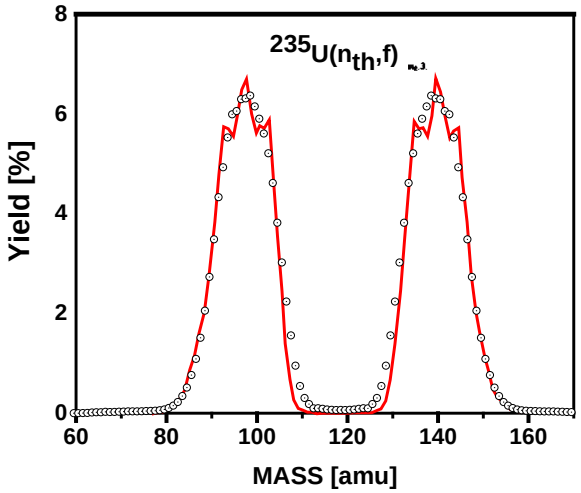

Fig. 4. Comparison of measured mass yield (dots) with data (solid line) taken from Ref.[4].

For calculations the successive approximation procedure to obtain pre-PFN emission mass described in Ref. [3] was used.

3 PFN data analysis

Measurement of PFN time-of-flight in present experiment was done using cathode pulse of TIC as a “T-zero” signal and the ND signal as “Stop” signal. The signals were digitized with 250 MHz sampling rate and stored during experiment for further off-line data analysis. Time difference between these two signals was analyzed implementing standard constant fraction time marking (CFTM) algorithm both to the cathode and to the ND waveforms. The realization of the algorithm described in Ref. [9] and was applied to the cathode waveform. The copy of the original signal is delayed by approximately 0.4 of the cathode signal rise time (~1000 ns) and summed with scaled and inverted original signal. The "T-zero" time is assigned to the crossing point of resulting signal with time axis. The crossing point was calculated using parabola interpolation between two successive samples, first of which has positive and second the negative values. The time mark for the ND signal was found in the similar way. It should be noted that to achieve the best timing resolution in CFTM realization one should convert sampled waveform to continuous form using Shannon's sampling formula [9]. Unless we do not deal with energy spectrum reconstruction, the resolution (~2.5 ns) provided in this simple implementation we found sufficient for PFN analysis. The neutron multiplicity was estimated by counting the number of coincidence between cathode pulse and PFN signal of ND. Due to high gamma radiation background both from the target and surrounding materials the PFN counts need to be separated from the gamma radiation using pulse shape analysis as described in Ref. [9].

The PFN detected by ND mainly is emitted from FF moving towards the ND, but the probability, that it was emitted by FF moving in opposite direction (complementary FF) is not zero and these events should be considered as the background. The background created by the complementary FF was investigated in Ref. [5] and was slightly modified in our approach. According to the reaction kinematics depicted in Fig. 2, the kinetic energy of the second FF in the CMF, must be much higher than the kinetic energy of the first FF. Bearing in mind the exponential drop of the PFN energy spectrum in the CMF, the contribution to the PFN from both FFs could be evaluated using the probabilities defined as:

$$W_x = 1/(1+\exp(E_{CM}^x - E_{CM}^y)),$$
$$W_y = \exp(E_{CM}^x - E_{CM}^y)/(1+\exp(E_{CM}^x - E_{CM}^y)), \quad (5)$$

where W_x, W_y - are probabilities of PFN emission with CM kinetic energies $E_{CM}^{x,y}$ of FF and its complement respectively. A comparison of the mass distributions plotted using measured data and probabilities, defined by eq. (5) are similar to Ref. [3], where the background from the complementary fragments for ^{252}Cf(SF) was found to be small.

The angular distribution of PFN emitted in FF CM reference frame is plotted in Fig. 5, proving that almost all of the PFN are emitted from fully accelerated FFs. The transformation from the LAB to CM reference frame was done using the following formula:

$$\cos(\Theta_{CM}) = (v_n^{Lab} \cdot \cos(\Theta) - v_1^F)/v_{CM}. \quad (6)$$

4 PFN analysis in ^{235}U(n_{th},f) reaction

The PFN distribution was evaluated considering neutron emission from the fully accelerated FF, using the reference frame moving along with the FF towards the ND. We used the Jacobian factor and conversion formulae from CM to LAB reference frame as was described in Ref. [10]:

$$\bar{\nu}(A,TKE) = \int_0^\infty \frac{Yc(A,TKE,V_{LAB}) \cdot V_{CM} \cdot (V_{LAB} - V_F \cdot \cos(\Theta))}{\varepsilon(V_{LAB}) \cdot V_{LAB}^2} dV_{LAB} / Y(A,TKE), \quad (7)$$

where $Y_C(A,TKE,V_{LAB})$ - the number of FF coincidences with ND, $\varepsilon(V_{LAB})$ is the ND efficiency dependence on PFN velocity in LAB frame, V_{LAB} - the PFN velocity measured in LAB frame, V_F - FF fragment velocity in LAB frame, V_{CM} is the PFN velocity in CM frame.

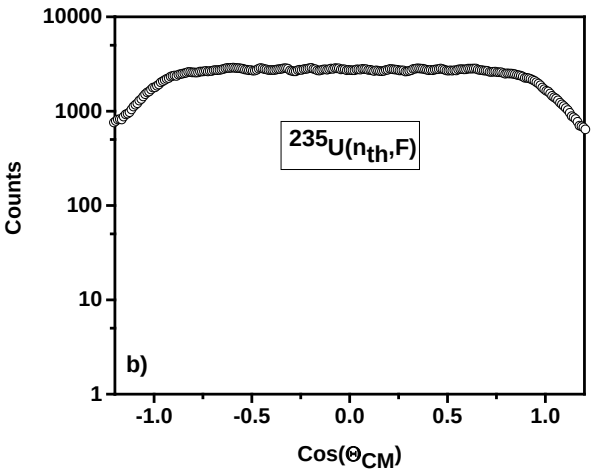

Fig. 5. The angular distribution of PFN emission measured in the FF CM frame.

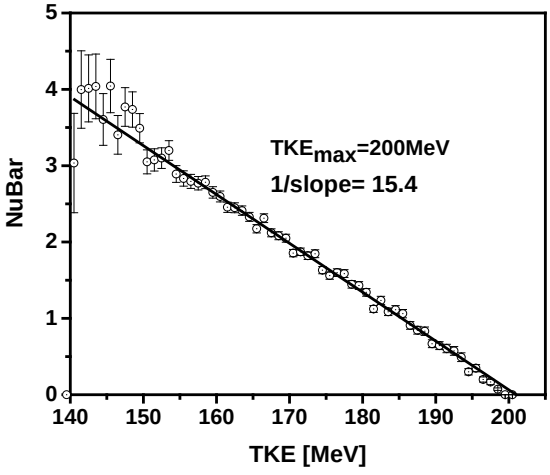

Fig. 6. The average PFN emission distribution mass dependence, measured in ^{235}U(n_{th},f) reaction in comparison with data from Ref. [7].

The distribution $Y(A,TKE)$ calculated without demanding coincidence with ND as was described above, but distribution $Yc(A,TKE,V_{LAB})$ calculated with FF energy corrected due to FF recoil after PFN emission as was described in Ref. [12].

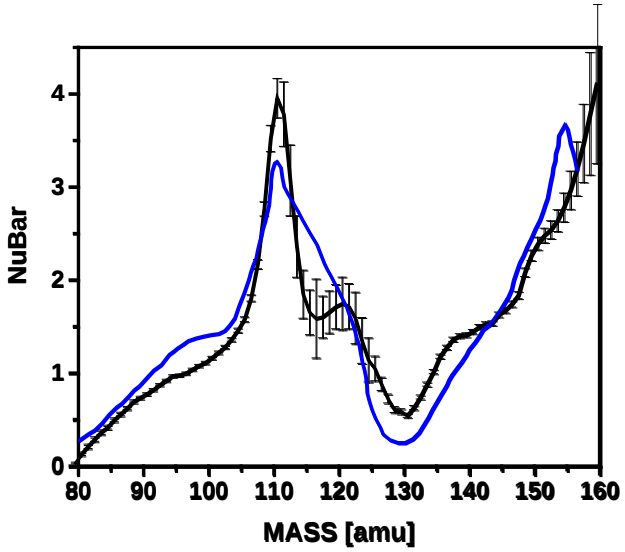

Fig. 7. The average PFN emission distribution dependence on FF TKE, measured in $^{235}U(n_{th},f)$ reaction with Q_{max}= ~205 MeV.

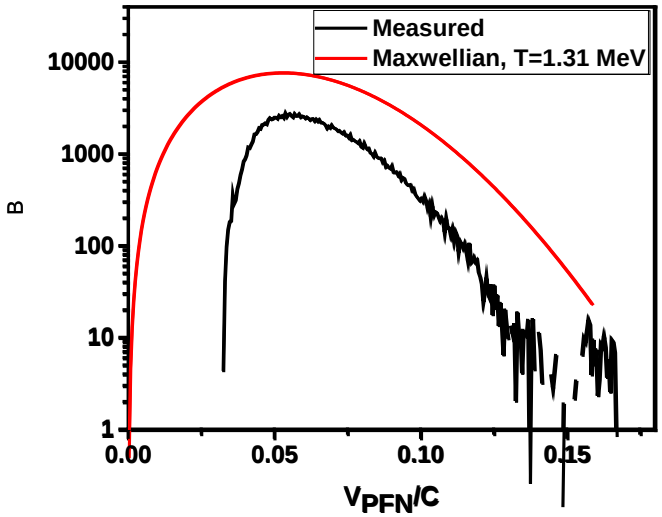

Fig. 8. Comparison of PFN velocity distribution, measured in $^{235}U(n_{th},f)$ reaction with Maxwell distribution with temperature parameter kT=1.31 MeV.

Dependence of average PFN multiplicity on TKE was evaluated in the similar manner using formulae (2) and plotted in Fig. 7. The PFN velocity distribution was evaluated from collected data and plotted in Fig. 8 along with the Maxwell distribution with temperature parameter T=1.313 MeV. The PFN detection efficiency was evaluated as the ratio of the measured PFN and plotted in Fig. 9.

It should be noticed that measurement of $\bar{\nu}(A)$ in $^{235}U(n_{th},f)$ was more complicated in comparison with $^{252}Cf(sf)$ due to very high peak to valley ratio in FF mass distribution for ^{235}U. Low statistics in the valley area of mass distribution makes data analysis very sensitive to background. That is why in this report we reanalyzed the data with the same data analysis software as was used in analysis of $^{235}U(n_{th},f)$ reaction. The test of our data analysis procedure in $^{252}Cf(sf)$ reaction was necessary for confidence in our results for $^{235}U(n_{th},f)$ which is more precisely reproduce mass distribution of the reaction.

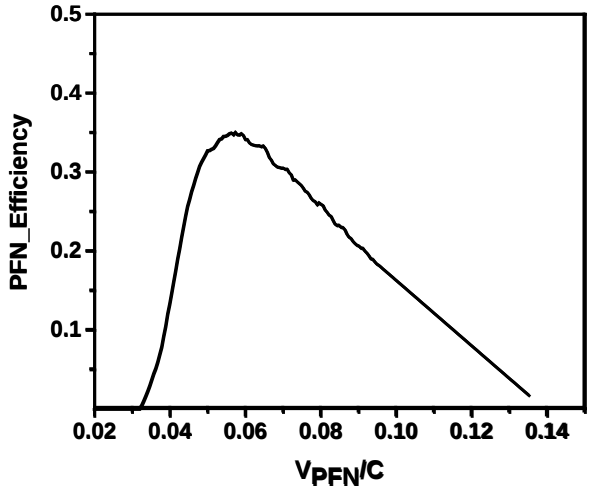

Fig. 9. PFN detection efficiency dependence on velocity measured in speed of light (C) units.

5 PFN analysis in $^{252}Cf(sf)$ reaction

Investigation of PFN in spontaneous fission of ^{252}Cf was done in 2007-2009 at IRMM with the experimental setup similar to presented in Fig.1. The ionization chamber was absolutely identical to the chamber used in above reported study. The PFN detectors were the same size

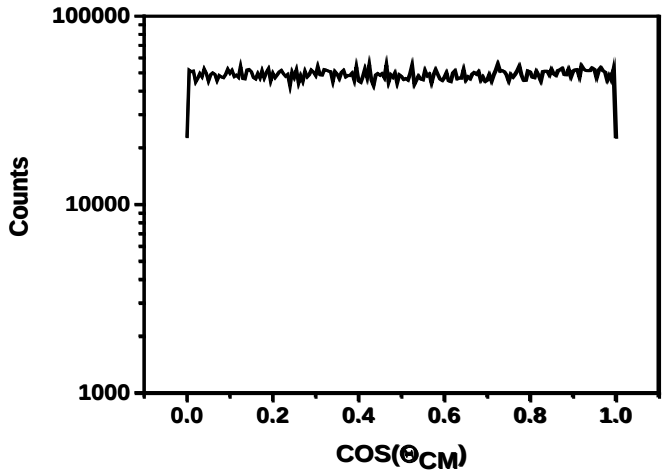

Fig. 10. PFN angular distribution for $^{252}Cf(sf)$ reaction in CM reference frame.

but in case of experiment with Cf-target the distance between target and PFN detector was 0.725 m. Measurement was done with data acquisition hardware and software was identical to reported above (except sampling frequency of WFD, which was 100 MHz). Data analysis was done using procedure as described above. The PFN angular distribution in CM reference frame was evaluated from data measured in laboratory reference frame and presented in Fig. 10. Cosine of angle between FF motion direction and PFN emission was evaluated using Eq. (6). The cosine distribution of neutron emission angle, measured in FF CM frame, was found to be almost homogeneous, proving that majority of PFN emitted from fully accelerated FF. Comparison of PFN velocity distribution with Maxwell distribution of PFN velocity is presented in Fig. 11.

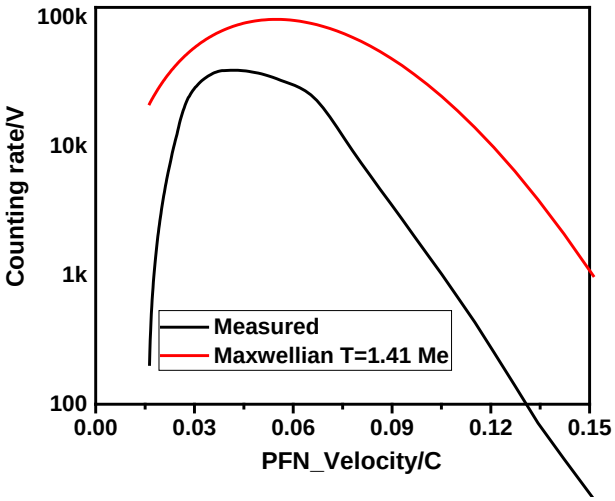

Fig. 11. Comparison of measured PFN velocity distribution with Maxwell distribution in ^{252}Cf(sf) experiment.

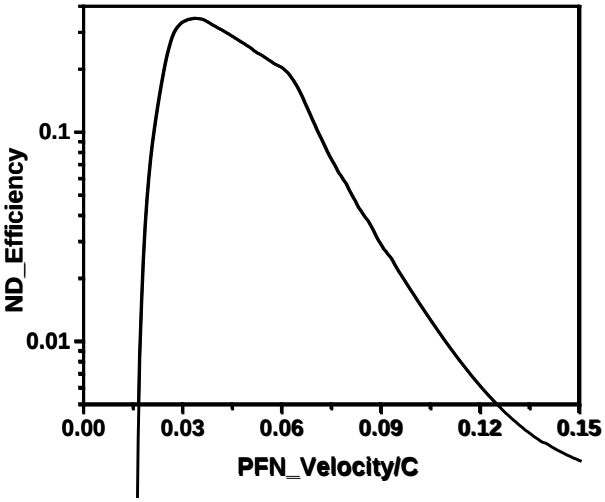

Fig. 12. PFN detection efficiency in reaction ^{252}Cf(sf) as function of the ratio of PFN speed, measured in units of speed-of-light (C).

The recommended value for temperature factor kT=1.41 MeV was used in this study. The PFN detection efficiency dependence on neutron velocity was evaluated as a ratio between measured PFN velocity distribution and Maxwell distribution. The dependence of PFN detection efficiency on the neutron speed presented in Fig. 12.

In both the ^{235}U(n_{th},f) and ^{252}CF(sf) experiments we implemented similar neutron-gamma separation procedure based on the difference between fast and slow scintillation decay time. Two values based on integrating the total charge over two different time periods conveyed information on the type of the detected particle. The plots in Fig. 13 demonstrate how the high and low kinetic energy region of PFN was separated from the background by increase of the threshold in total charge integral over longer time interval. It should be noted that the plots 1 and 2 in Fig. 13 were obtained without application of the neutron gamma separation criterion using only the threshold. The plot 3 was obtained with application of neutron-gamma separation criterion. It should be pointed out that in both experiments the background in PFN distribution was practically completely removed with the applied threshold value corresponding to PFN kinetic energy of ~0.5 MeV.

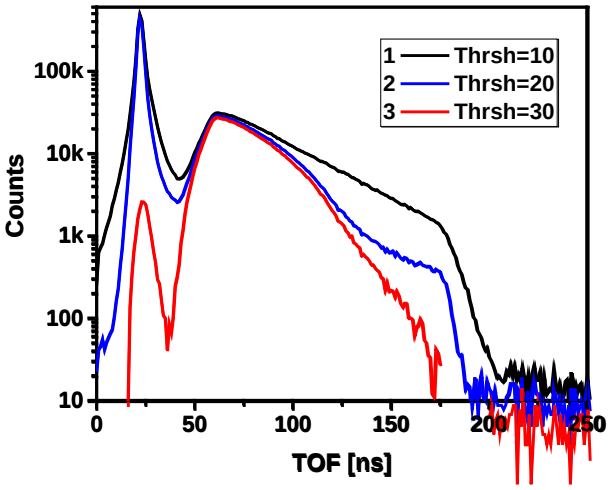

Fig. 13. Dependence of background in high and low PFN kinetic energy spectra on the threshold in total charge integrated over long time interval.

6 Conclusions and outlook

The average PFN emission was evaluated using the same data analysis software as was used in the analysis of $^{235}U(n_{th},f)$ reaction described in above section. Results of average PFN emission dependence on FF mass and TKE are presented in Fig. 14 and Fig. 15 respectively.

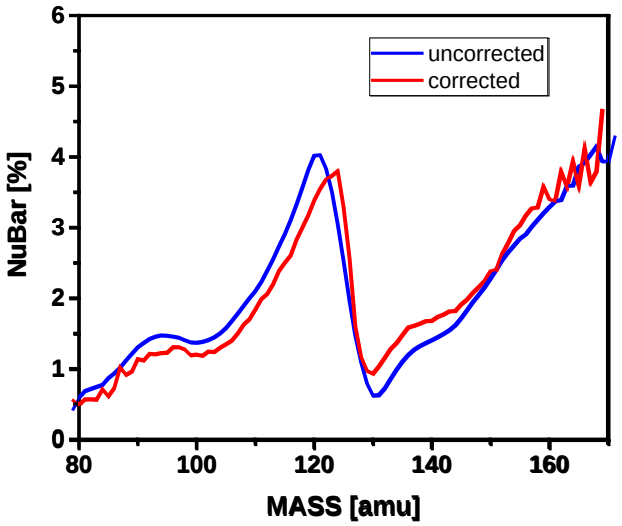

Fig. 14. Mass dependence of average PFN emission in ^{252}Cf(sf).

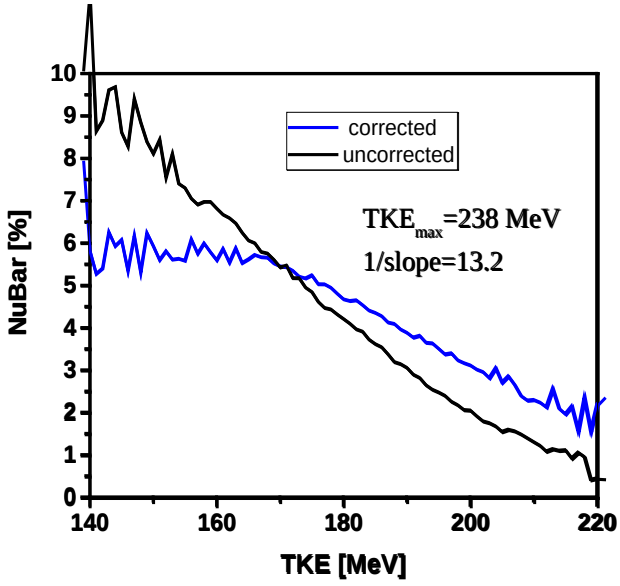

Fig. 15. $\bar{\nu}(TKE)$ dependence in ^{252}Cf(sf) reaction. The maximum TKE release, when PFN emission became impossible PFN indicated in figure.

The distributions presented for FF recoil taken into account and ignored in order to demonstrate the effects of corrections according to Ref. [11]. It should be noted that the average neutron number also should be corrected according to formula (11) from Ref. [11].

We found this correction very small both in $^{235}U(n_{th},f)$ and $^{252}Cf(sf)$ reactions in full agreement with Ref. [11]. The difference between uncorrected and corrected distributions on Fig. 14 was quite significant, which we explain with formula (4) used for pulse height correction due to Frisch-grid inefficiency. Detailed description and derivation of the formula can be found in research paper [8]. As was pointed out in review paper [12], the use of large

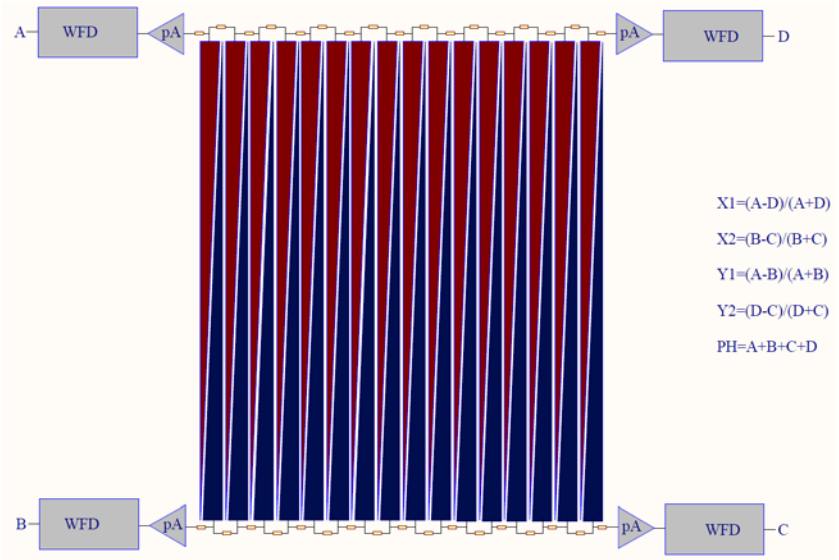

Fig. 16. One of the anodes of position sensitive twin ionization chamber.

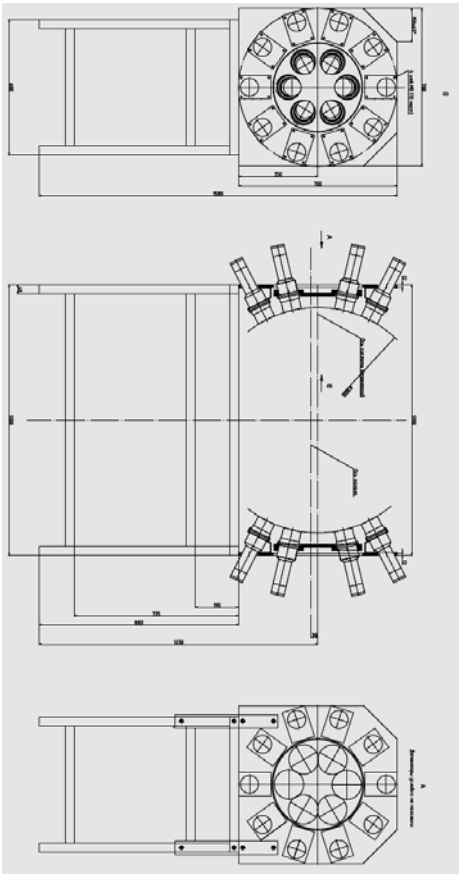

Fig. 17. Fast neutron detector composed of 32 liquid scintillation modules with position sensitive twin ionization chamber in centre (not shown in figure).

neutron detectors (with higher PFN detection efficiency) in many aspects was preferable in PFN investigations. Bearing this in mind we started investigations, which would combine the properties of both detectors with high and low efficiency. Before development of new experimental setup for PFN we have developed position sensitive twin fission chamber with capability of reconstruction the orientation of fission axis in 3D [13]. The twin chamber consisted of common cathode, where fissile target can be located. Two segmented anodes located at 40 mm distance symmetrically from the both sides of the cathode plane plain. Segmented anodes consisted of triangular strips, electrically isolated from each other as demonstrated in Fig. 16. Each strip as shown in the figure connected to the nodes of the resistive chain filter. Operational principle of position sensitive ionization chamber, formulae for FF "charge centre-of gravity" and FF orientation evaluation was provided in Refs. [8,13]. Fast neutron detector consisted of 32 type VS-0499-100 scintillation detector modules of diameter 76 mm and 51 mm from SCIONIX HOLLAND BV (Fig. 17). The setup was planned to use in experiment to the end of this year at IREN –resonance neutron source in Dubna.

Acknowledgements

Authors express their gratitude to Liudmila Mytsyna for help in preparation the manuscript for publication in ISINN26 proceedings.

References

1. A.A. Naqvi, F. Kappeler, and F. Dickmann, Phys. Rev. **C34**, 218 (1986).
2. A. Al-Adili, D. Tarrio, F.-J. Hambsch, A. Gook, K. Jansson, A. Solders, V. Rakopoulos, C. Gustavson, M. Lantz, A. Materrs, S. Oberstedt, A.V. Prokofiev, M. Viladi, M. Osterlund, and S. Pomp, *EPJ Web of Conferences* **122**, 01007 (2016).
3. C. Budtz-Jorgensen and H.-H. Knitter, Nucl. Phys., **A490**, 307 (1988).
4. C. Wagemans, *The Nuclear Fission Process*, CRC Press, Boca Raton, FL, 1991.
5. S. Zeynalov, O. Zeynalova, F.-J. Hambsch and S. Oberstedt, Bull. Russ. Acad. Sci.: Phys. **73**,506 (2009).
6. Zeynalov, S., Hambsch, F.-J., Oberstedt, S., 2011. Jour. Korean Phys. Soc. **59**, 1396.
7. V.F. Apalin, Yu. N. Gtitsuk, I.E. Kutikov, V.I. Lebedev, and L.A. Mikaelyan, Nucl. Phys., **55**, 249 (1964).
8. O. Zeynalova, Sh. Zeynalov, M. Nazarenko, F.-J. Hambsch, and S. Oberstedt, *AIP Conf. Proc*. **1404**, 325(2011).
9. G. Knoll, *Radiation Detection and Measurement*, John Willey & Sons, Inc, Third edition, 2001.
10. H.R. Bowman, J.C.D. Milton, S.G. Thompson, and W.J. Swiatecki, Phys. Rev. **129** (1963) 2133.
11. A. Gavron, Nucl. Instrum. and Meth., **115** (1974) 99.
12. H. Nifenecker, C. Signarbieux, R. Babinet, J. Poitou, *Neutron and gamma emission in fission*, IAEA-SM-174/207.
13. Sh. Zeynalov, P. Sedyshev, O. Sidorova, V. Shvetsov, Applications of Nuclear Techniques (CRETE17), *International Journal of Modern Physics: Conference Series*, Vol. **48** (2018) 1860123.